ACS APPLIED MATERIALS & INTERFACES

Research Article

www.acsami.org

Tuning the Friction Characteristics of Gecko-Inspired Polydimethylsiloxane Micropillar Arrays by Embedding Fe_3O_4 and SiO_2 Particles

Ye Tian,[†,‡] Zizhou Zhao,[‡] Gina Zaghi,[‡] Yongkwan Kim,[‡] Dongxing Zhang,[†] and Roya Maboudian*[,‡]

[†]School of Materials Science and Engineering, Harbin Institute of Technology, Harbin 150001, China

[‡]Department of Chemical and Biomolecular Engineering, University of California, Berkeley, California 94720, United States

Supporting Information

ABSTRACT: In order to improve stiffness of polydimethylsiloxane (PDMS) pillars while maintaining high friction, the effects of embedding Fe_3O_4 and SiO_2 particles on the friction behavior of PDMS micropillars are studied. Both types of added particles increase the stiffness of the PDMS composite, but affect the friction behavior differently. The frictional force of the fibrillar array fabricated with Fe_3O_4/PDMS composite decreases initially, then increases as the particle content increases. For silica/PDMS composite pillars, the frictional force is independent of the particle density. Characterization by scanning electron microscopy shows that Fe_3O_4 particles are distributed uniformly in the PDMS matrix at low concentration, but heterogeneous distribution is observed at high particle loading, with particles being hindered from penetrating into the pillars. For silica/PDMS composite pillars, the particles distribute homogeneously inside the pillars, which is attributed to the formation of hydrogen bonding between silica particles and PDMS. The difference in particle distribution behavior is used to explain the observed difference in the friction response of these two composite systems.

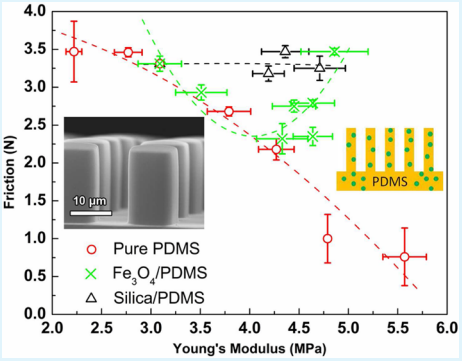

KEYWORDS: *friction, Young's modulus, PDMS, micropillar, gecko-inspired adhesives*

1. INTRODUCTION

The ability of geckos to strongly adhere to and rapidly detach from surfaces is attributed to a complex array of hierarchical microfibers and nanofibers on their toes.[1] These hairy structures ensure a high area of contact between the feet and the counter-surface, maximizing the interfacial attraction.[2,3] Over the past decade, potential applications in residue-free tapes, medical adhesives,[4] high friction surfaces,[5] material transport,[6] and climbing robots[7] have motivated research interest in the fabrication and testing of synthetic adhesives that mimic some characteristics of gecko adhesion.[8−15] In designing such adhesives, the stiffness of the material (as indicated by the Young modulus) is a critical consideration, because it determines the flexibility of the fiber elements and ultimately the aspect ratio of the fibers required to achieve the desired adhesive strength. Although the number of studies that experimentally investigated the effect of material stiffness is limited, the increase in Young modulus is associated with a decrease in adhesion.[16−18]

So far, the tuning of the Young modulus of fiber arrays has been mostly realized by changing the stiffness of the bulk material, for example, by varying the precursor ratio or the curing time of the elastomers.[16,17] In this study, we examine an alternative way to modify the stiffness of fibrillar adhesives by embedding particles in polydimethylsiloxane (PDMS). Many gecko adhesives fabricated to date are made of PDMS, because of its simple curing procedure, high flexibility, and chemical inertness.[8] Composite material of particles in PDMS has been widely explored to achieve improvement in the material properties,[19−22] but their potential application in gecko adhesives has been shown only very recently, for example, in achieving magnetically actuated adhesion with embedded iron particles in PDMS flaps[6] and enhancing adhesion by incorporating gold particles into the tip of PDMS microfibers.[23] Although these studies have demonstrated interesting applications of the particle−PDMS composite in gecko-inspired adhesives, the influence of the nanoparticles on the stiffness and the adhesive performance have not been examined in detail.

By mixing in various weight percentages of Fe_3O_4 and SiO_2 particles into PDMS prior to curing in a silicon template, the stiffness of the resulting microfiber array is varied and the effect on the macroscale friction is monitored. We find that, although Young modulus monotonically increases as the particle weight percentage increases, the friction behavior is more complex and the heterogeneity of the particle distribution within the PDMS can be critical in determining the friction performance of the micropillar array.

Received: December 30, 2014
Accepted: June 4, 2015
Published: June 4, 2015

DOI: 10.1021/acsami.5b03301
ACS Appl. Mater. Interfaces 2015, 7, 13232−13237

2. EXPERIMENTAL DETAILS

Template Fabrication. The template consists of an array of square holes in silicon obtained by deep reactive-ion etching through a mask defined by photolithography. A 4 in. Si(100) wafer is rinsed by deionized water and coated with a positive photoresist (Fujifilm OCG 825). A photomask is prepared by attaching a plastic mesh (McMaster-Carr) covered by 100 μm of evaporated Cr to a blank photomask. The stepper used for exposure (Model GCA 6200−USH-350DP) reduces the mask pattern by a factor of 10, resulting in 10 μm-square hole array. After exposure and development, the wafer is etched by alternating pulses of SF_6 and C_4F_8 plasma, which produces vertical holes in silicon. The photoresist is removed by oxygen plasma. For easy separation after molding, the template is reacted with an octadecyltrichlorosilane antisticking monolayer, as described previously.[24] The wafer is diced into 1 cm × 1 cm chips, and cleaned by sonication in acetone and isopropanol for 15 min each, followed by blow drying with nitrogen.

PDMS Curing in Silicon Template. The PDMS resin (Dow Corning) is first mixed with either silica nanoparticles (Sigma−Aldrich, nominally ∼7 nm in size, resulting in the aggregate effective size of 100−250 nm[25,26]) or synthetic black iron oxide particles (Alpha Chemicals, ∼300 nm) and sonicated for 15 min. After introducing a curing agent into the mixture with a curing agent:resin weight ratio of 1:10, an additional 15 min of sonication is performed, followed by degassing in a vacuum chamber to eliminate any bubbles. After all visible bubbles disappear, the mixture is poured onto the silicon template, followed by another degassing for removing any bubbles introduced during the pour (Figure 1). The amount of the mixture poured over the template is adjusted to keep the constant sample thickness of 130 μm. The samples are cured at 60 °C for 16 h and peeled off.

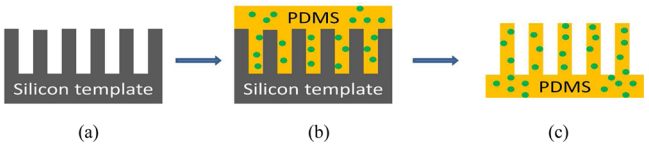

Figure 1. Schematic diagram of the process for fabricating particle-embedded PDMS pillars from silicon templates: (a) silicon template with an array of square holes, (b) mixture of PDMS and particles poured onto silicon templates, and (c) cured PDMS pillars with particles once peeled from silicon templates.

The PDMS modulus can also be varied by mixing the PDMS base resin with varying mass ratio of the PDMS curing agent. Here, the mass ratio of curing agent to PDMS base resin is varied from 0.075 to 0.125. The mixture is sonicated for 15 min, followed by degassing in a vacuum chamber to eliminate bubbles. After all visible bubbles disappear, the mixture is poured onto silicon templates, followed by another degassing to remove any bubbles introduced during the pour. The samples are cured at 60 °C for 16 h and peeled off. The thickness of the sample is 130 μm.

Friction Testing. The friction of the patch is measured against a glass slide (VWR) using a standard pulley setup, described previously.[24] A normal load of ∼0.18 N is distributed over the sample using a soft rubber patch for consistent contact, and weight is progressively added to the pulley until the sample detaches from the glass. Each sample is tested five times, and the run with the highest friction is recorded. Between each run, the glass slide is rinsed with acetone and wiped dry, and the sample is cleaned with isopropanol and blow-dried with nitrogen.

Young Modulus Measurements. Thick (∼6 mm) PDMS or particle/PDMS composite samples are prepared and the stiffness of sample is measured with a Type A shore durometer (Intercomp), according to ASTM Standard D2240. Each sample is tested several times at different locations and the average shore A value is used to estimate the Young modulus of the material using the relationship shown below:[27]

$$E\ (\mathrm{N/mm^2}) = \frac{1-\mu^2}{2RC_3}\left(\frac{C_1 + C_2 Sh_A}{100 - Sh_A}\right) \quad (1)$$

where C_1, C_2, and C_3 are constants with values of 0.549 N, 0.07516 N, and 0.025 mm, respectively; R is the radius of the durometer's indenter (R = 0.395 mm); μ the Poisson's ratio (estimated to be μ = 0.50[28,29]); and Sh_A is the shore A value of the material.

3. RESULTS AND DISCUSSION

The conventional method to tune the Young modulus of elastomers involves changing the mass ratio of the base resin to the curing agent.[16,17,30,31] We have prepared microfiber array samples with various concentrations of curing agent as a control case, in order to later provide a comparison with regard to mechanical and friction properties with PDMS embedded with different types and concentrations of particles. The curing temperature affects the Young modulus, structure, and performance of PDMS.[17] In this study, the curing temperature of 60 °C is chosen for PDMS and the composites. The relationship between the friction behavior of adhesive patch and Young modulus of PDMS with different mass ratio of the curing agent to the PDMS base is displayed in Figure 2. As the

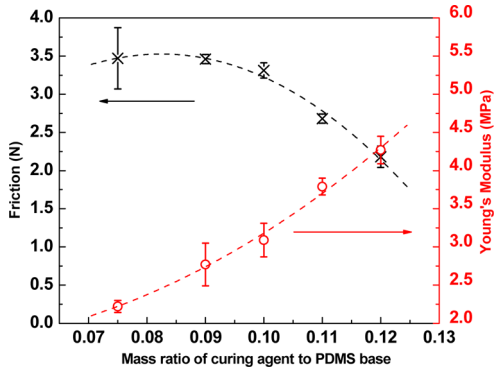

Figure 2. Friction (black crosses) and Young modulus (red circles) as a function of mass ratio of the PDMS curing agent to PDMS base resin. The lines are drawn to guide the eyes. Sample size = 1 cm × 1 cm.

amount of curing agent increases, the Young modulus of the cured PDMS increases significantly, from 2.22 MPa to 4.27 MPa. Because the curing agent is responsible for cross-linking the siloxane oligomers in the base resin, the increased amount of curing agent is consistent with a higher degree of polymer cross-linking and a correspondingly higher stiffness,[32,33] which is consistent with a previous study.[34]

Figure 2 shows that the ratio of curing agent to PDMS base resin also significantly affects the friction performance of the samples. As the ratio increases, the frictional force of the pillars decreases sharply, from 3.5 N to 2.2 N. This decline in friction can be attributed to two factors. As the curing agent component is increased, the actual contact between the top of the pillars and the counter-surface is reduced, because of the increased stiffness of the pillars. In addition, the bending flexibility of the pillar elements is reduced as the material stiffness increases, causing fewer pillars to come in contact across the entire sample. As such, an inverse trend is observed between the friction and stiffness, as a function of the added curing agent.

Increasing the amount of curing agent in the PDMS pillars enhances the Young modulus, but sacrifices the friction of sample. In order to obtain improved stiffness and also retain

DOI: 10.1021/acsami.5b03301
ACS Appl. Mater. Interfaces 2015, 7, 13232−13237

high friction, Fe_3O_4 and SiO_2 particles with different contents are incorporated into PDMS pillars. The Young modulus and the frictional force of PDMS pillar array with different weight percentages of embedded Fe_3O_4 are plotted in Figure 3. The

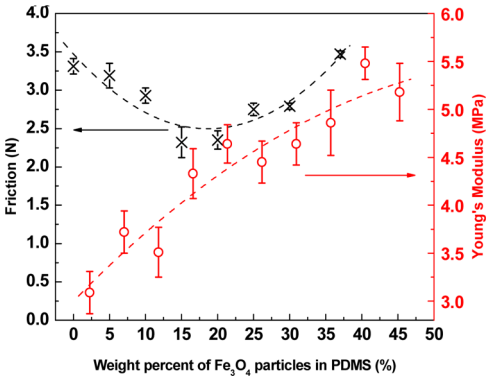

Figure 3. Friction behavior (black crosses) and Young modulus (red circles) of Fe_3O_4/PDMS composite with various weight percentages of Fe_3O_4 particles. The lines are drawn to guide the eyes.

mass ratio of the curing agent to PDMS base is fixed at 1:10. As the concentration of Fe_3O_4 increased, the Young modulus of the composite monotonically increases. Young modulus of a composite material (E_c) can be approximated by the following formula:[35]

$$E_c = V_m E_m + V_p E_p \quad (2)$$

where V_m is the volume fraction of the matrix, V_p the volume fraction of the particles, E_m the Young modulus of the matrix, and E_p is the Young modulus of the particles. Because the Young modulus of the Fe_3O_4 particles is larger than that of the PDMS, the Young modulus of the composite is expected to increase as the volume fraction of the Fe_3O_4 particles in PDMS increases.

However, the resulting friction behavior is observed to be more complex. When the weight percentage of Fe_3O_4 in PDMS is <20%, the friction force of Fe_3O_4/PDMS pillars decreases as the Fe_3O_4 content increases. When the weight percentage of Fe_3O_4 is >25%, the frictional force of the composite pillars is enhanced by increasing the concentration of Fe_3O_4. The initial decrease in friction can be explained by the increased stiffness with the addition of increasing amounts of Fe_3O_4 particles. Similar to the case where the material stiffness was varied by additional curing agent, an increase in stiffness may reduce both the number of pillars in contact with the glass counter-surface and the interfacial surface area between each pillar and glass.

To help explain the counterintuitive trend above 25 wt %, SEM images are employed to observe and compare the particle distribution at low and high Fe_3O_4 concentrations. Figure 4 shows SEM images of PDMS pillars embedded with 15 wt % Fe_3O_4 particles. It can be observed that the particles are distributed uniformly inside of pillars as well as in the backing. The embedding of Fe_3O_4 particles into PDMS can reduce friction by preventing direct contact of the top pillar surface with the glass.

SEM images of 35 wt % Fe_3O_4/PDMS samples are shown in Figure 5, going from the pillars (Figure 5a) to the backing region adjacent to the pillars (Figure 5b) to the other side of the polymer backing (Figure 5c). The results indicate that statistically the concentration of Fe_3O_4 particles in the backing

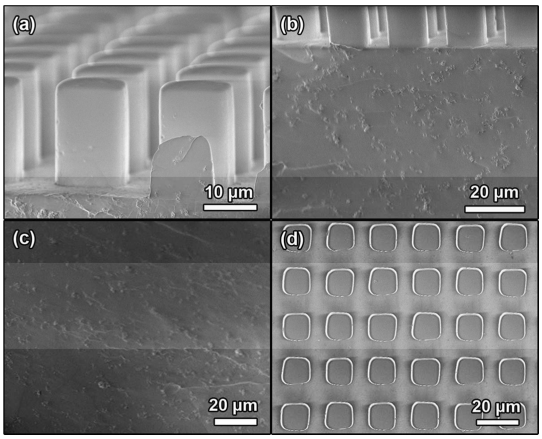

Figure 4. SEM images of 15 wt % Fe_3O_4/PDMS composite pillars: (a) cross-sectional view of the pillars part, (b) cross-sectional view of the backing adjacent to the pillars, (c) cross-sectional view of the bottom of backing part, and (d) top view of the pillars.

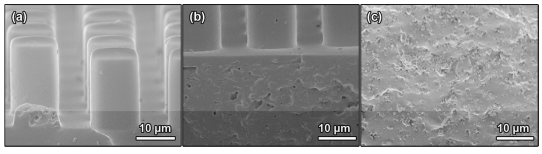

Figure 5. SEM images of 35 wt % Fe_3O_4/PDMS composite pillars: (a) cross-sectional view of the pillars part, (b) cross-sectional view of the backing adjacent to the pillars, and (c) cross-sectional view of the bottom of backing part.

adjacent to pillars is less than that observed in the backing bottom. The images indicate that the particles distribute nonuniformly in the material. Based on these results, we present the following hypothesis. It is observed that the viscosity of the Fe_3O_4/PDMS mixture increases as the weight percentage of Fe_3O_4 exceeds 20%. This, in turn, may hinder the dispersion of the particles to form homogeneous composite pillars. In particular, this may be the case inside the pillars, given that the cross-sectional area of each pillar is 10 μm × 10 μm (Figure 4d) with a length of 20 μm, while the backing part of the adhesive is much thicker. Thus, we hypothesize that the Fe_3O_4 particles in high viscosity polymer mixture are hindered from diffusing into the pillars. As such, for large Fe_3O_4 loading, the top region of the pillars may remain soft, because of the reduced density of Fe_3O_4 particles in that region. Because the frictional force is mainly dependent on the top surface of pillars, the softer pillar top results in increased friction performance, as observed in Figure 3 with the content of Fe_3O_4 particles above 20%.

This hypothesis is further verified by atomic force microscopy (AFM) (Digital Instrument Multimode Nanoscope IIIA) characterization of Fe_3O_4/PDMS composites. AFM images (Figure S1 in the Supporting Information) show that the roughness of the top surfaces of the pillars is different for various loadings of Fe_3O_4 particles. The top surface of the PDMS pillar without any Fe_3O_4 particles is relatively smooth, with a root-mean-square roughness (RMS) of ~5 nm. After incorporating 15 wt % Fe_3O_4 particles into PDMS, the top surface of the composite pillar becomes rougher (RMS ≈ 100 nm), which is attributed to the particles on the surface region of the pillar. As the amount of Fe_3O_4 particles reaches 35 wt %, the roughness of the top surface of the pillar decreases (RMS ≈

DOI: 10.1021/acsami.5b03301
ACS Appl. Mater. Interfaces 2015, 7, 13232−13237

46 nm). This behavior is consistent with the SEM results and the discussions above, which helps to explain why the friction of Fe_3O_4/PDMS composite pillars decreases at first and then increases with the increasing concentration of Fe_3O_4 particles.

To test another type of embedded particles with a potentially more uniform mixture, the incorporation of SiO_2 particles, which are chemically more similar to PDMS, into PDMS was investigated. Because SiO_2 particles several nanometers in size are unstable, they aggregate to form larger particles with an effective size of ~100−250 nm.[25,26] Figure 6 exhibits the

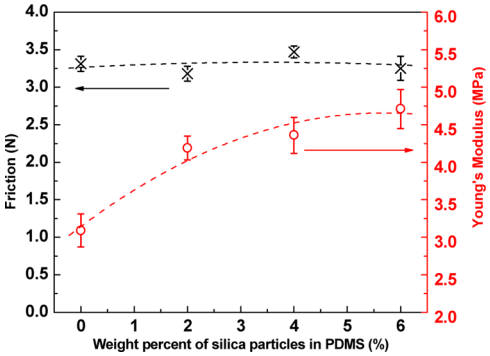

Figure 6. Friction behavior (black crosses) and Young modulus (red circles) of silica/PDMS composite with various contents of silica particles. The solid lines are drawn to guide the eyes.

friction behavior and Young modulus of silica/PDMS composite pillars, as a function of weight percent of silica particles. The mass ratio of curing agent to PDMS base is fixed at 1:10. Similar to the case with Fe_3O_4, the Young modulus is again increased as the amount of silica (which is much stiffer than PDMS) is increased. This phenomenon is induced by the strong interaction between the silica and PDMS.[36] However, compared with Fe_3O_4/PDMS composite pillars, the friction behavior of silica/PDMS pillars is different. As the weight percent of silica in PDMS pillars increases, the friction forces remain constant, indicating that the friction property of silica/PDMS composite is independent of the weight content of silica particles in the composite.

The representative SEM images of PDMS pillars embedded with silica are displayed in Figure 7. It can be observed that the

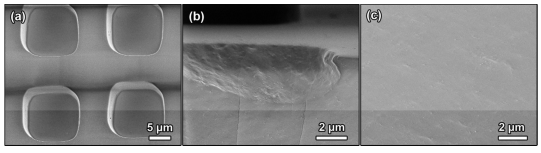

Figure 7. SEM images of 6 wt % silica/PDMS composite pillars: (a) top view, (b) cross-sectional view of the backing adjacent to the pillars, and (c) cross-sectional view of the bottom of backing part.

top surface is smooth (Figure 7a), and no obvious agglomerate phenomenon is exhibited in the backing adjacent to the pillars (Figure 7b) and the bottom of backing part (Figure 7c), indicating that silica particles are embedded in PDMS pillars and distributed homogeneously in the system. This is also confirmed by AFM analysis, as shown in Figure S2 in the Supporting Information, indicating a smooth surface with an RMS value of 35 nm. It is well-known that the silica has a highly porous structure, and the physical characteristics of fumed silica/PDMS composite is not only affected by the total surface area of silica, but also by pore volume of silica.[37] Because of the large surface area of fumed silica particles (~400 m^2/g), the behavior of fumed silica is dependent on the surface silanol functional groups and the surface siloxane bond.[25] The interaction between the surface silanol groups of the oxide skeleton chains and the oxygen atoms of PDMS surface induces a strong physical absorption and hydrogen bonding between fumed silica particles and PDMS.[25] Once silica particles are embedded in PDMS, although some of particles might agglomerate, the size of aggregates is still small. Furthermore, we hypothesize that the interaction between PDMS and silica—in particular, the formation of "bound rubber" on silica surface comprised of polymer molecules[36]—leads to silica particles being covered by PDMS. Thus, the silica particles are distributed uniformly throughout the sample. Also, the top surface of the pillars remains essentially soft, even as more silica particles are added. PDMS coverage on top of the pillars, as well as the homogeneous distribution of silica particles in PDMS, maintains the high frictional performance.

Figure 8 summarizes frictional performance as a function of Young modulus for the PDMS pillars modified by the three

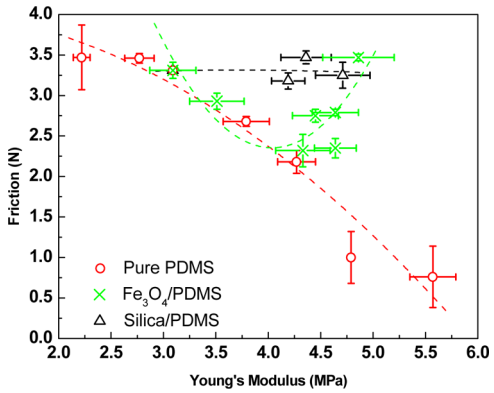

Figure 8. Relationship between friction and Young modulus of the three types of PDMS pillars in this study. Red circles represent PDMS pillars with different weight percent curing agent, green crosses correspond to Fe_3O_4/PDMS composite, and black triangles represent silica/PDMS composite. The curves are drawn to guide the eyes.

ways discussed, namely, by varying the amount of curing agent and incorporating stiff Fe_3O_4 and silica particles that increase the Young modulus of the PDMS matrix. While a high curing agent ratio and stiff particles can increase the Young modulus of the pillars, their influence on the friction is different. For PDMS with an increased mass ratio of curing agent, Young modulus increases and the friction force decreases sharply, because of the reduced bending flexibility of pillars. For PDMS embedded with an increasing content of Fe_3O_4 particles, the frictional force first decreases, because of an increase in the stiffness of composite pillars, and then increases because of the heterogeneous distribution of the Fe_3O_4 particles, hindering their incorporation inside the pillars and causing the top region of the pillars to remain soft. By embedding silica in PDMS, the Young modulus of the pillars increases but the frictional force stays at the same level, which is attributed to the reaction between the PDMS matrix and the silica particles, which allows PDMS to cover the particles and keep the top region of the pillars soft.[38]

DOI: 10.1021/acsami.5b03301
ACS Appl. Mater. Interfaces 2015, 7, 13232−13237

4. CONCLUSION

Young modulus and friction behavior of Fe_3O_4/PDMS and silica/PDMS composite pillars tailored for varied particle concentrations are studied. The particles embedded in PDMS pillars increase Young modulus of the pillars, but different effects on the friction behaviors are observed. For Fe_3O_4/PDMS composite pillars, the frictional force initially decreases with the increased density of particles, and recovers with further addition of particles. In the case of silica particles in PDMS, the resulting frictional force is maintained at a relatively high level, independent of the density of silica particles. This is attributed to the uniform distribution of the silica particles in PDMS and their coverage with PDMS on the pillar tops.

The results show that, by embedding particles in PDMS pillars, the frictional force can be tuned while increasing the Young modulus. Compared with PDMS pillars with varying curing agent, embedding stiff particles in PDMS pillars can keep the frictional force relatively high while the stiffness is increased. This may be useful in the practical design of synthetic gecko adhesives, since they are often limited in performance, because of fiber clumping.[5] The modulus of pillars with particles can be increased while adhesion and friction remain relatively unaffected, which can allow the fabrication of longer pillars without the potential problem of pillar clumping or collapse due to low stiffness.

■ ASSOCIATED CONTENT

Ⓢ Supporting Information

Figure S1 shows AFM images of the top surface of Fe_3O_4/PDMS composite pillars with different loadings of Fe_3O_4 particles: (a) PDMS pillar without any Fe_3O_4 with a scan size of 2.5 μm × 2.5 μm (RMS ≈ 5 nm), (b) 15 wt % Fe_3O_4 in PDMS composite pillar with a scan size of 6.0 μm × 6.0 μm (RMS ≈ 100 nm), and (c) 35 wt % Fe_3O_4 in PDMS composite pillar with a scan size of 4.0 μm × 4.0 μm (RMS ≈ 46 nm). The z-range is 410 nm. Figure S2 shows an AFM image of the top surface of 6 wt % SiO_2/PDMS composite pillar with a scan size of 6.0 μm × 6.0 μm (RMS ≈ 35 nm) and z-range of 410 nm. The Supporting Information is available free of charge on the ACS Publications website at DOI: 10.1021/acsami.5b03301.

■ AUTHOR INFORMATION

Corresponding Author

*E-mail: maboudia@berkeley.edu.

Notes

The authors declare no competing financial interest.

■ ACKNOWLEDGMENTS

This work was supported by National Science Foundation Grant Nos. EEC-0832819 (through the Center of Integrated Nanomechanical Systems) and DMR-1207053. Y.T. was also supported, in part, by the Chinese Scholarship Council through a graduate fellowship.

■ REFERENCES

(1) Autumn, K.; Liang, Y. A.; Hsieh, S. T.; Zesch, W.; Chan, W. P.; Kenny, T. W.; Fearing, R.; Full, R. J. Adhesive Force of a Single Gecko Foot-Hair. *Nature* **2000**, *405*, 681−685.

(2) Autumn, K.; Sitti, M.; Liang, Y. C. A.; Peattie, A. M.; Hansen, W. R.; Sponberg, S.; Kenny, T. W.; Fearing, R.; Israelachvili, J. N.; Full, R. J. Evidence for Van Der Waals Adhesion in Gecko Setae. *Proc. Natl. Acad. Sci. U.S.A.* **2002**, *99*, 12252−12256.

(3) Arzt, E.; Gorb, S.; Spolenak, R. From Micro to Nano Contacts in Biological Attachment Devices. *Proc. Natl. Acad. Sci. U.S.A.* **2003**, *100*, 10603−10606.

(4) Kwak, M. K.; Jeong, H. E.; Suh, K. Y. Rational Design and Enhanced Biocompatibility of a Dry Adhesive Medical Skin Patch. *Adv. Mater.* **2011**, *23*, 3949−3953.

(5) Lee, D. H.; Kim, Y.; Fearing, R. S.; Maboudian, R. Effect of Fiber Geometry on Macroscale Friction of Ordered Low-Density Polyethylene Nanofiber Arrays. *Langmuir* **2011**, *27*, 11008−11016.

(6) Gillies, A. G.; Kwak, J.; Fearing, R. S. Controllable Particle Adhesion with a Magnetically Actuated Synthetic Gecko Adhesive. *Adv. Funct. Mater.* **2013**, *23*, 3256−3261.

(7) Yu, J.; Chary, S.; Das, S.; Tamelier, J.; Pesika, N. S.; Turner, K. L.; Israelachvili, J. N. Gecko-Inspired Dry Adhesive for Robotic Applications. *Adv. Funct. Mater.* **2011**, *21*, 3010−3018.

(8) Boesel, L. F.; Greiner, C.; Arzt, E.; del Campo, A. Gecko-Inspired Surfaces: A Path to Strong and Reversible Dry Adhesives. *Adv. Mater.* **2010**, *22*, 2125−2137.

(9) Sameoto, D.; Menon, C. Recent Advances in the Fabrication and Adhesion Testing of Biomimetic Dry Adhesives. *Smart Mater. Struct.* **2010**, *19*, 103001.

(10) del Campo, A.; Arzt, E. Design Parameters and Current Fabrication Approaches for Developing Bioinspired Dry Adhesives. *Macromol. Biosci.* **2007**, *7*, 118−127.

(11) Jeong, H. E.; Suh, K. Y. Nanohairs and Nanotubes: Efficient Structural Elements for Gecko-Inspired Artificial Dry Adhesives. *Nano Today* **2009**, *4*, 335−346.

(12) Kwak, M. K.; Pang, C.; Jeong, H. E.; Kim, H. N.; Yoon, H.; Jung, H. S.; Suh, K. Y. Towards the Next Level of Bioinspired Dry Adhesives: New Designs and Applications. *Adv. Funct. Mater.* **2011**, *21*, 3606−3616.

(13) Hu, S. H.; Xia, Z. H. Rational Design and Nanofabrication of Gecko-Inspired Fibrillar Adhesives. *Small* **2012**, *8*, 2464−2468.

(14) Jagoda, A.; Hui, C. Y. Adhesion, Friction, and Compliance of Bio-Mimetic and Bio-Inspired Structured Interfaces. *Mater. Sci. Eng., R.* **2011**, *72*, 253−292.

(15) Lin, J.; Yang, Q. L.; Xu, J. J.; Liu, K. S.; Guo, L.; Jiang, L. Adhesive Materials Inspired by Gecko and Mussel. *Prog. Chem.* **2012**, *24*, 1946−1954.

(16) Li, M.; Zhao, A. W.; Jiang, R.; Wang, D. P.; Li, D.; Guo, H. Y.; Tao, W. Y.; Gan, Z. B.; Zhang, M. F. Regulation of the Elastic Modulus of Polyurethane Microarrays and Its Influence on Gecko-inspired Dry Adhesion. *Appl. Surf. Sci.* **2011**, *257*, 3336−3340.

(17) Greiner, C.; Buhl, S.; del Campo, A.; Arzt, E. Experimental Parameters Controlling Adhesion of Biomimetic Fibrillar Surfaces. *J. Adhes.* **2009**, *85*, 646−661.

(18) Puthoff, J. B.; Prowse, M. S.; Wilkinson, M.; Autumn, K. Changes in Materials Properties Explain the Effects of Humidity on Gecko Adhesion. *J. Exp. Biol.* **2010**, *213*, 3699−3704.

(19) Xu, R. Q.; Lu, Y. Q.; Jiang, C. H.; Chen, J.; Mao, P.; Gao, G. H.; Zhang, L. B.; Wu, S. Facile Fabrication of Three-Dimensional Graphene Foam/Poly(dimethylsiloxane) Composites and Their Potential Application as Strain Sensor. *ACS Appl. Mater. Interfaces* **2014**, *6*, 13455−13460.

(20) Li, Z.; Nambiar, S.; Zheng, W.; Yeow, J. T. W. PDMS/Single-Walled Carbon Nanotube Composite for Proton Radiation Shielding in Space Applications. *Mater. Lett.* **2013**, *108*, 79−83.

(21) Liu, G. P.; Xiangli, F. J.; Wei, W.; Liu, S. N.; Jin, W. Q. Improved Performance of PDMS/Ceramic Composite Pervaporation Membranes by ZSM-5 Homogeneously Dispersed in PDMS via a Surface Graft/Coating Approach. *Chem. Eng. J.* **2011**, *174*, 495−503.

(22) Nakata, K.; Kimura, H.; Sakai, M.; Ochiai, T.; Sakai, H.; Murakami, T.; Abe, M.; Fujishima, A. UV/Thermally Driven Rewritable Wettability Patterns on TiO_2−PDMS Composite Films. *ACS Appl. Mater. Interfaces* **2010**, *2*, 2485−2488.

(23) Téllez, J. P. D.; Harirchian-Saei, S.; Li, Y.; Menon, C. Adhesion Enhancement of Biomimetic Dry Adhesives by Nanoparticle in Situ Synthesis. *Smart. Mater. Struct.* **2013**, *22*, 105031.

DOI: 10.1021/acsami.5b03301
ACS Appl. Mater. Interfaces 2015, 7, 13232−13237

(24) Kim, Y.; Limanto, F.; Lee, D. H.; Fearing, R. S.; Maboudian, R. Role of Counter-Substrate Surface Energy in Macroscale Friction of Nanofiber Arrays. *Langmuir* **2012**, *28*, 2922−2927.
(25) Paquien, J. N.; Galy, J.; Gérard, J. F.; Pouchelon, A. Rheological Studies of Fumed Silica−Polydimethylsiloxane Suspensions. *Colloids Surf., A* **2005**, *260*, 165−172.
(26) Camenzind, A.; Schweizer, T.; Sztucki, M.; Pratsinis, S. E. Structure and Strength of Silica-PDMS Nanocomposites. *Mater. Res. Soc. Symp. Proc.* **2011**, *1312*, 241−246.
(27) Kunz, J.; Studer, M. Determining the Modulus of Elasticity in Compression via the Shore A Hardness. *Kunststoffe Int.* **2006**, *96*, 92−94.
(28) Bendall, S. J.; Graz, I.; Lacour, P. S. Zinc Oxide Nanowire Rigid Platforms on Elastomeric Substrates. *ACS Appl. Mater. Interfaces* **2011**, *3*, 3162−3166.
(29) Yin, J.; Yague, L. J.; Boyce, C. M.; Gleason, K. K. Biaxially Mechanical Tuning of 2-D Reversible and Irreversible Surface Topologies through Simultaneous and Sequential Wrinkling. *ACS Appl. Mater. Interfaces* **2014**, *6*, 2850−2857.
(30) Tchoquessi Diodjo, M. R.; Belec, L.; Aragon, E.; Joliff, Y.; Lanarde, L.; Perrin, F. X. Silane Coupling Agent for Attaching Fusion-Bonded Epoxy to Steel. *ACS Appl. Mater. Interfaces* **2013**, *5*, 6751−6761.
(31) Wang, Z.; Volinsky, A. A.; Gallant, N. D. Crosslinking Effect on Polydimethylsiloxane Elastic Modulus Measured by Custom-Built Compression Instrument. *J. Appl. Polym. Sci.* **2014**, *131*, 41050.
(32) Wilbur, J. L.; Jackman, R. J.; Whitesides, G. M.; Cheung, E. L.; Lee, L. K.; Prentiss, M. G. Elastomeric Optics. *Chem. Mater.* **1996**, *8*, 1380−1385.
(33) Campbell, D. J.; Beckman, K. J.; Calderon, C. E.; Doolan, P. W.; Ottosen, R. M.; Ellis, A. B.; Lisensky, G. C. Replication and Compression of Surface Structures with Polydimethylsiloxane Elastomer. *J. Chem. Educ.* **1999**, *76*, 537−541.
(34) Song, F. C.; Ren, D. C. Stiffness of Cross-Linked Poly-(dimethylsiloxane) Affects Bacterial Adhesion and Antibiotic Susceptibility of Attached Cells. *Langmuir* **2014**, *30*, 10354−10362.
(35) GE, X.; Schmauder, S. Elastic Modulus and Interface Stress Constraint of Particle Reinforced Composites. *Mater. Sci. Eng., A* **1993**, *168*, 93−97.
(36) Levresse, P.; Feke, D. L.; Manas-Zloczower, I. Analysis of the Formation of Bound Poly(dimethylsiloxane) on Silica. *Polymer* **1998**, *39*, 3919−3924.
(37) Shim, S. E.; Isayev, A. I. Rheology and Structure of Precipitated Silica and Poly (dimethyl siloxane) System. *Rheol. Acta* **2004**, *43*, 127−136.
(38) Delebecq, E.; Hamdani-Devarennes, S.; Raeke, J.; Cuesta, J. M. L.; Ganachaud, F. High Residue Contents Indebted by Platinum and Silica Synergistic Action during the Pyrolysis of Silicone Formulations. *ACS Appl. Mater. Interfaces* **2011**, *3*, 869−880.

DOI: 10.1021/acsami.5b03301
ACS Appl. Mater. Interfaces 2015, 7, 13232−13237